A Novel Unspecific Peroxygenase from Galatian marginata for Biocatalytic Oxyfunctionalization Reactions

Ma, Yunjian; Liang, Hongjing; Zhao, Zexin; Wu, Bin; Lan, Dongming; Hollmann, Frank; Wang, Yonghua

DOI
10.1016/j.mcat.2022.112707

Publication date
2022

Document Version
Final published version

Published in
Molecular Catalysis

Citation (APA)
Ma, Y., Liang, H., Zhao, Z., Wu, B., Lan, D., Hollmann, F., & Wang, Y. (2022). A Novel Unspecific Peroxygenase from Galatian marginata for Biocatalytic Oxyfunctionalization Reactions. *Molecular Catalysis*, *531*. https://doi.org/10.1016/j.mcat.2022.112707

Molecular Catalysis 531 (2022) 112707

Contents lists available at ScienceDirect

Molecular Catalysis

journal homepage: www.journals.elsevier.com/molecular-catalysis

A Novel Unspecific Peroxygenase from *Galatian marginata* for Biocatalytic Oxyfunctionalization Reactions

Yunjian Ma [a,b], Hongjing Liang [c], Zexin Zhao [d], Bin Wu [c], Dongming Lan [a,*], Frank Hollmann [e,*], Yonghua Wang [a,f,*]

[a] School of Food Science and Engineering, South China University of Technology, Guangzhou 510640, China
[b] Neher's Biophysics Laboratory for Innovative Drug Discovery, State Key Laboratory of Quality Research in Chinese Medicine, Macau University of Science and Technology, Taipa, Macau, China
[c] School of Bioscience and Bioengineering, South China University of Technology, Guangzhou 510006, China
[d] Key Laboratory of Fermentation Engineering (Ministry of Education), Hubei Key Laboratory of Industrial Microbiology, Hubei University of Technology, Wuhan 430068, PR China
[e] Department of Biotechnology, Delft University of Technology, van der Maasweg 9, 2629HZ, Delft, The Netherlands
[f] Guangdong Youmei Institute of Inteligent Bio-manufacturing Co., Ltd, Foshan, Guangdong 528200, China

ARTICLE INFO

Keywords:
Unspecific peroxygenase
Galerina marginata
Bioinformatics analysis
Heterologous expression
Oxyfunctionalization

ABSTRACT

Unspecific peroxygenases (UPOs, EC 1.11.2.1) are promising oxyfunctionalization catalysts because of their unique stereoselectivity. However, so far only a few UPOs have been reported. In this study, gene mining was used to identify a gene from *Galerina marginata* that coded for a novel UPO (*Gma*UPO). *Gma*UPO was expressed in *Pichia pastoris* X-33 by scale-up fermentation (the UPO activity of the culture supernatant was 118 U/L). *Gma*UPO exhibited a molecular weight of 40 kDa and exhibited highest activity at 35°C and pH 9, respectively. Furthermore, *Gma*UPO was demonstrated to catalyze the epoxidation, sulfoxidation, and hydroxylation of common substrates, particularly fatty acids such as tridecanoic acid. The molecular basis for *Gma*UPO regioselectivity for fatty acid hydroxylation was explored by molecular modelling. The regioselectivity was mostly governed by the architecture of the enzyme's active site.

1. Introduction

Unspecific peroxygenases (UPOs, E. C. 1.11.2.1) are increasingly being recognized as 'dream catalysts' for the selective oxyfunctionalization of non-activated C-H bonds [1–4]. As heme-thiolate enzymes, UPOs, like the well-known P450 monooxygenases [5–7], use catalytically active oxyferryl-species (Compound I) to activate inert C-H bonds (**Scheme 1**). Mechanistically, UPO reactions follow the hydrogen peroxide shunt pathway of the P450 catalytic cycle [3]. As a result, UPOs directly utilize partially reduced O_2 in form of H_2O_2 or organic hydroperoxides rather than reductively activating O_2 (as P450 monooxygenases do) within the enzyme active site. This difference in catalytic mechanism translates into a simpler molecular architecture of UPOs and highly simplified reaction schemes. Whilst P450 monooxygenases require a stoichiometric supply of reducing equivalents from NAD(P)H, which is provided to the heme active site directly via a series of single-electron transfer steps, UPOs are regenerated directly with H_2O_2.

Intriguingly, only a few UPOs are currently available for practical use. Hager in the 1960s discovered the chloroperoxidase from *Caldariomyces fumago* (*Cfu*CPO) [8–9]. Hofrichter and coworkers more recently revealed the UPO from *Agrocybe aegerita* (*Aae*UPO) [10–14]. Of note, relatively few new UPOs have been added to the organic chemistry toolbox [15]. Some new UPOs have been isolated from cultures of wild-type *Coprinellus radians* [16], *Marasmius rotula* [17–18], *Marasmius wettsteinii* [19], *Candolleomyces aberdarensis* (*syn. Psathyrella aberdarensis*), *Coprinopsis verticillata* and *Chaetomium globosum* [20–21].

Pioneering work by Alcalde and coworkers paved the way for the next step of UPO research by developing recombinant expression systems for UPOs [22–23] in well-established fungal expression systems such as *Saccharomyces cerevisiae* and *Pichia pastoris* enabling large-scale cultivation [24] and engineering of new UPOs [23,25-33]. Also recombinant expression of UPOs in prokaryotic hosts such as *Escherichia coli* is possible [34–35]. Other research groups world-wide have accepted the challenge on broadening the scope of UPOs available for

* Corresponding authors at: Department of Biotechnology, Delft University of Technology, Van der Maasweg 9, 2628BL Delft, Netherlands.
E-mail addresses: dmlan@scut.edu.cn (D. Lan), f.hollmann@tudelft.nl (F. Hollmann), yonghw@scut.edu.cn (Y. Wang).

https://doi.org/10.1016/j.mcat.2022.112707
Received 4 August 2022; Received in revised form 18 September 2022; Accepted 19 September 2022
Available online 30 September 2022

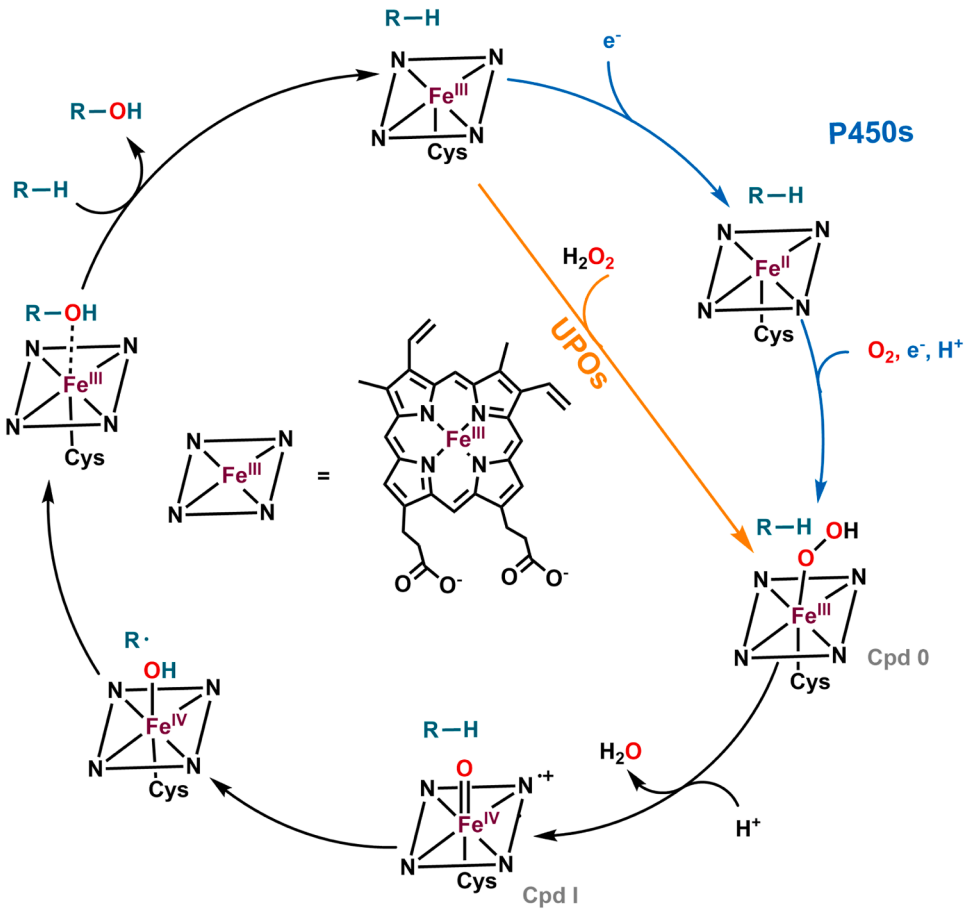

Scheme 1. Comparison of the catalytic mechanisms of peroxygenases (UPOs) and P450 monooxygenases. Both enzyme classes utilize the so-called compound I (Cpd I) as active species to mediate H-atom abstraction from the starting material (R-H) followed by fast capture of the resulting alkyl radical forming the hydroxylated product. Cpd I itself is generated from so-called compound 0 (Cpd 0) via dehydration. In case of P450 monooxygenases, Cpd 0 is formed in a sequence of two individual single electron transfer steps and O_2 binding to the half-reduced heme-complex. Peroxygenases form Cpd 0 directly from the resting state and H_2O_2.

organic oxyfunctionalization reactions [36–41].

Despite the impressive advances in UPO research over the last decade, it appears that we have merely scratched the surface thus far. A recent analysis of 800 fungal genomes identified more than 1900 putative UPO genes [42], demonstrating the discrepancy between scope and current availability of novel UPOs.

To (partially) address this gap, we chose the putative UPO gene from *Galerina marginata* for expression and further characterization of the gene product (*Gma*UPO) in the present study (**Figure 1**).

2. Materials and Methods

2.1. Chemical reagents and materials

All chemicals were purchased from TCI, Aladdin and Sigma-Aldrich in the highest purity available and used without further treatment. *Pichia pastoris* X33 and pPICZαB vector were obtained from the Guangdong Youmei Institute of Intelligent Bio-manufacturing Co., Ltd (Foshan, Guangdong, China). *Escherichia coli* DH5α competent cells were purchased from Weidi Biotechnology Co., Ltd (Guangzhou, China). Restriction enzymes EcoRI and SalI were purchased from Takara Dalian bioengineering company (Dalian, China). The Seamless cloning kit was purchased from Zhongmei Taihe Biotechnology Co., Ltd (Beijing, China), and the Plasmid extraction kit and the 12.5% SDS-PAGE color preparation kit were purchased from Sangong Bioengineering Co., Ltd (Shanghai,China). A mouse anti-his tag monoclonal antibody was used as the primary antibody for Western blotting, while the secondary antibody was a goat anti-mouse IgG (H&L) secondary antibody (HRP marker); both antibodies were purchased from Jinruisi biotechnology company.

The unspecific peroxygenase from *Agrocybe aegerita* (*Aae*UPO) used in this study was obtained from a previous pilot-scale production of this enzyme [24].

2.2. Bioinformatics analysis of GmaUPO

The protein FASTA sequence (KDR72024.1) was download from NCBI (https://www.ncbi.nih.gov.in). The DNAMAN software and the Multalin website were used to align the sequence of *Gma*UPO gene with a series of other reported UPO genes and examine their homology. Protein properties such as theoretical molecular weight, isoelectric point, total overall average hydrophilicity coefficient, and instability coefficient were predicted using ExPASy (https://web.expasy.org/protparam).

2.3. Preparation of GmaUPO

2.3.1. Construction of GmaUPO expression engineered bacteria

The *Gma*UPO gene sequence (KDR72024.1) was synthesized by Sangong Bioengineering Co., Ltd (Shanghai, China). *Gma*UPO gene fragment was acquired using PCR amplification (**Table S1**). The amplification conditions were 98°C for 5 min then (98°C for 15 s, 55°C for 15 s and 72°C for 30 s) for 50 cycles, and lastly 72°C for 5 min. Pure pPICZαB vector was digested by the enzymes *Eco* RI and *Sal* I, then transferred to *E. coli* DH5α competent cells and plated on LB solid medium (25 μg/mL zecoin) at 37°C for 12-16 h. Single colonies were selected into 5 ml liquid LB medium with zecoin at a final concentration of 25 μg/mL and cultured for 12-16 h at 37°C and 200 rpm. Plasmid identity was confirmed by plasmid isolation and sequencing.

The recombinant plasmid pPICZαB was linearized, electrically converted into *Pichia pastoris* X33 competent cells, and plated on YPG solid medium (100 μg/mL zeocin) at 30°C for 36-48 h. A single colony (<

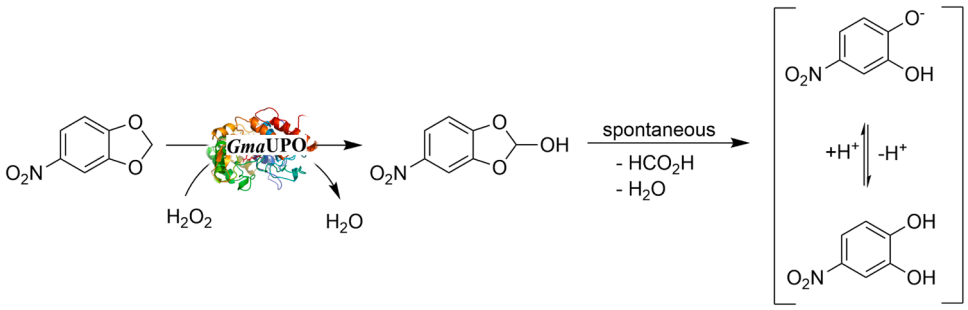

Scheme 2. NBD oxidation to detect *Gma*UPO peroxygenase activity.

1mm diameter) was selected into a 5 ml YPG liquid medium (100 μg/mL zeocin) and cultured for 16-18 h at 30°C and 220 rpm.

2.3.2. Recombinant expression of GmaUPO

A positive monoclonal strain (*@pPICZαB-SPgma-Gma*UPO) was inoculated into a 100 mL YPG liquid medium containing 100 μg/mL zeocin and cultured in a shaker for 24 h at 30°C, 240 rpm. This served as inoculum (3% v/v) in a 350 ml YPG liquid medium and was cultured for about 12-16h at 30°C and 250 rpm until the OD_{600} reached more than 10.

The bioprocesses were carried out in a BIOTECH-7JG-3 bioreactor (Shanghai Baoxing bio-engineering) filled with 3 L basal salt medium (26.7 mL/L phosphoric acid, 1.176 g/L $CaSO_4$, 18.2 g/L K_2SO_4, 14.9 g/L $MgSO_4{\cdot}7H_2O$, 4.35g/L KOH, 40 g/L glycerol) supplemented with 4.35 mL/L PTM1 trace salts (6 g/L $CuSO_4{\cdot}5H_2O$, 0.08 g/L NaI, 3 g/L $MnSO_4{\cdot}H_2O$, 0.2 g/L $Na_2MoO_4{\cdot}2H_2O$, 0.02 g/L H_3BO_3, 0.5 g/L $CoCl_2$, 20 g/L $ZnCl_2$, 65 g/L $FeSO_4{\cdot}7H_2O$, 0.2 g/L Biotin, 5 mL/L H_2SO_4). The pH was set to 5.0 and maintained using NH_4OH. Following DO calibration, the fermentation batch phase was initiated by inoculating 350 mL of seed culture, with process parameters set to 30°C, air press 0.05 Mpa, dissolved oxygen concentration held above 30%, and organic silicon antifoam injected automatically via a level sensor. The original glycerol in the basal salt medium was completely consumed after 16 h, resulting in a significant increase in the dissolved oxygen concentration. The glycerol feeding phase began immediately. The feeding solution contained 70% (m/v) glycerol and 12 mL/L PTM1 trace salt solution, and the process parameters were automatically adjusted to maintain a DO of 20 %. When the cell concentration reached around 180-220 g/L, the glycerol feeding was halted, and the temperature and pH were set to 22°C and 5.5, respectively. The 'methanol feeding phase' was initiated by adding methanol containing 12 mL/L PTM1 trace salt solution. The DO was kept at 40 % for the next 168 h of cultivation by regulating the airflow into the culture medium. Finally, the cell culture was clarified via centrifugation. The supernatant was used for further investigations.

2.4. Biochemical characterization of GmaUPO

2.4.1. Western blot and SDS-PAGE analysis

Protein samples from the gel were electrically transferred onto a 0.2 μm polyvinylidene difluoride membrane (PVDF) for western blot analysis. The membrane was blocked at room temperature with 5% skimmed milk powder and then treated with a polyclonal mouse anti-His-tag antibody and rabbit anti-mouse HRP labeled antibody to confirm the presence of recombinant *Gma*UPO protein. The SDS-PAGE analysis used 12.5% SDS-PAGE color preparation kit.

2.4.2. Enzyme activity determination

To measure oxyfunctionalisation activity, we employed the classical peroxygenase assay based on NBD oxidation [43]. The specific method was performed as follows: 100 μL phosphate buffer solution (100 mM, pH 7), 30 μL NBD (5 mM dissolved in 100% anhydrous acetonitrile), 20 μL deionized water, and 30 μL enzyme solution were added to the 96 well plates, and 20 μL 100 mM H_2O_2 was then added to start the reaction. An absorption of 425nm was measured after 5 min (**Scheme 2**). In addition, the enzyme solution was inactivated by high temperature as the experimental control, while the buffer solution served as the blank control. All experiments were conducted in three parallel groups.

Enzyme activity was measured in units U, where 1 U is the amount of *Gma*UPO required to convert NBD to 1 μM 4-nitrocatechol in 1 min at 25°C and pH 7. The following formula was used to calculate enzyme activity (1-1).

$$X = \frac{n}{t} \tag{1-1}$$

X represents *Gma*UPO enzyme activity, U/L;
n represents the concentration of 4-nitroctechol produced, μM;
t represents reaction time, min.

2.4.3. Temperature dependency of GmaUPO

To examine the reliance of *Gma*UPO activity on the reaction temperature, the NBD assay (2.4.2) was performed at different temperatures (25, 30, 35, 40, 45, and 50°C respectively).

The thermal stability of *Gma*UPO was assessed by incubating the enzyme solution at different temperatures (25, 30, 35, 40, 45, and 50°C), taking samples at regular intervals (0.5, 1, 2, 3, 4, 6, 8, 10 and 12 h), and evaluating the residual activity with the NBD-assay (2.4.2).

2.4.4. pH sensitivity dependency of GmaUPO

The pH sensitivity of *Gma*UPO was investigated using NBD as a substrate. Experimental methods for optimal reaction pH were as follows: the buffer solution in the enzyme activity reaction system was replaced with buffer solutions of 5, 6, 7, 8, 9, and 10 accordingly (citrate-phosphate pH 5, phosphate pH 6 and 7, Tris-HCl pH 8, pH 9 and 10 each at 100 mM concentration).

The pH stability of *Gma*UPO was determined by incubating the enzyme in buffers with different pH values (described above). Samples were taken and analyzed under standard conditions at regular intervals.

2.4.5. Metal ions sensitivity

*Gma*UPO enzyme solution (950 μL) was supplemented with 50 μL 100 mM metal salt solutions ($FeSO_4{\cdot}7H_2O$, $MnCl_2{\cdot}4H_2O$, $CuCl_2{\cdot}2H_2O$, $CaCl_2$, $CoCl_2{\cdot}6H_2O$, $FeCl_3$, $NiCl_2{\cdot}6H_2O$, $MgSO_4$ and EDTA, corresponding to 5 mM final concentrations of the metal ions) and incubated for 2 h at 4°C. The residual *Gma*UPO activity was measured using the above-mentioned standard assay.

2.4.6. Organic reagent sensitivity

*Gma*UPO enzyme solution (700 μL) was supplemented with 300 μL of methanol, ethanol, acetone, or DMSO, and incubated for 2 h at 4°C. The residual *Gma*UPO activity was measured using the above-mentioned standard assay.

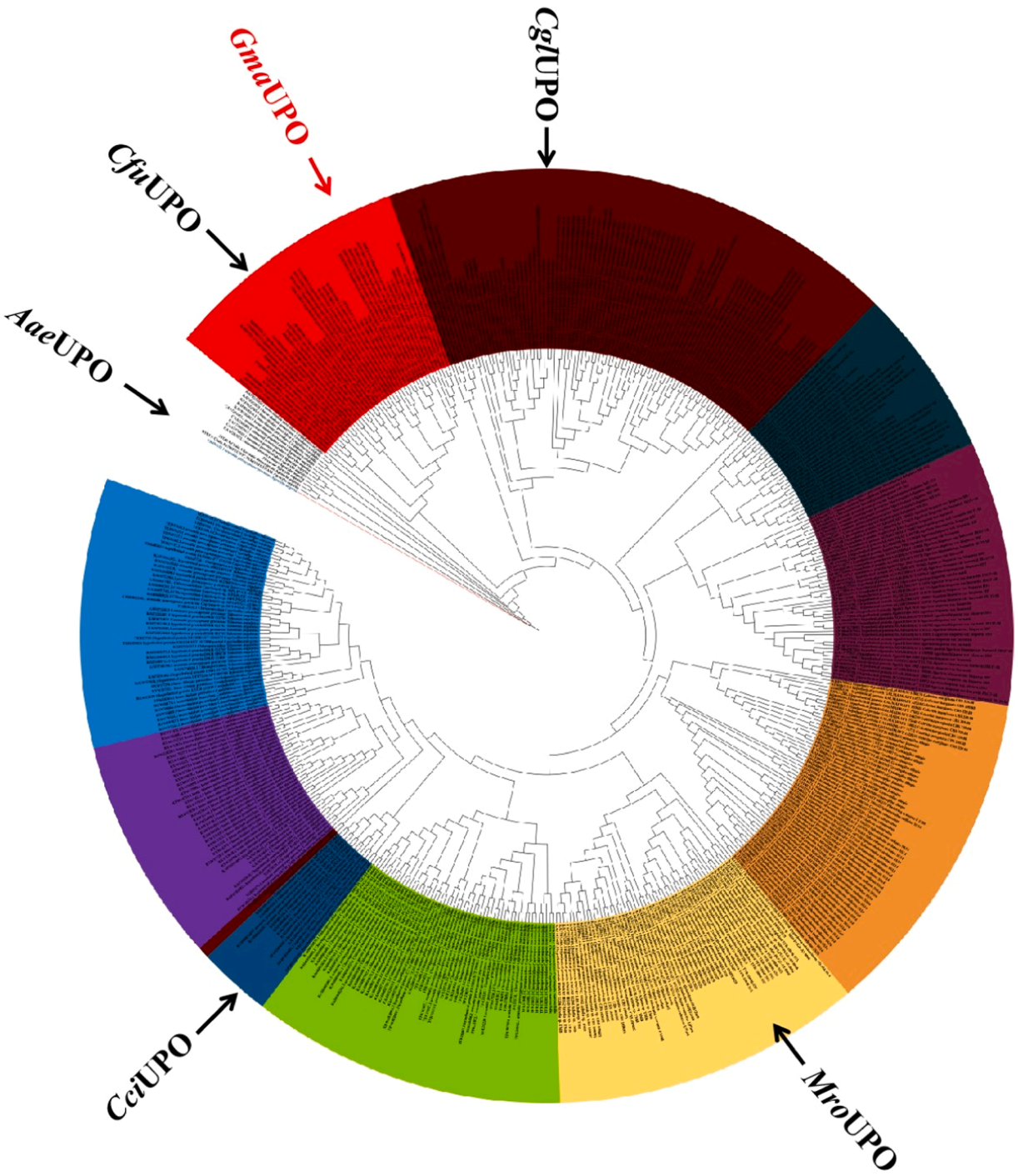

Fig. 1. Phylogenetic tree analysis of UPO genes and localization of *Gma*UPO. Also highlighted are the UPOs *Agrocybe aegerita* (*Aae*UPO), *Caldariomyces fumago* (*Cfu*UPO), *Chaetomium globosum* (*Cgl*UPO), *Marasmius rotula* (*Mro*UPO) and *Coprinopsis cinerea* (*Cci*UPO). For a full overview including sequences and accession numbers refer to the SI.

2.5. Experimental reactions of GmaUPO

Catalytic transformations involving *Gma*UPO were performed using a previously reported *in situ* H_2O_2 generation system based on the aerobic oxidation of choline using the Choline oxidase from *Arthrobacter nicotianae* (*An*ChOx) [44–46].

Reactions were performed at a 1 mL scale in sealed glass vials (4 mL volume) for 24 h at 30°C while shaking at 500 rpm. The reaction mixture (buffer: 50 mM NaPi, pH 7) contained 0.1 U *Gma*UPO, *An*ChOx (5 μM), Choline chloride (100 mM), and substrate (1 mM fatty acids and 10 mM in case of all other starting materials). The reactions were halted by adding 100 μL of HCl (0.3 M) and incubating for 5 mins at 500 rpm and room temperature. Fatty acids and their derivatives were extracted with methyl tert-butyl ether (MTBE, 1mL) and dried under Na_2SO_4. TMS-derivatization was achieved by treatment with N,O-bis (trimethylsilyl) trifluoroacetamide (BSTFA), analyzed on GC-MS. Other compounds were extracted with ethyl acetate (1 mL, using 25 mM dodecane as an internal reference), dried over Na_2SO_4, and evaluated on GC.

2.6. Gas chromatograph and temperature profiles

The GC-FID analysis was performed on an Agilent 7890B GC system

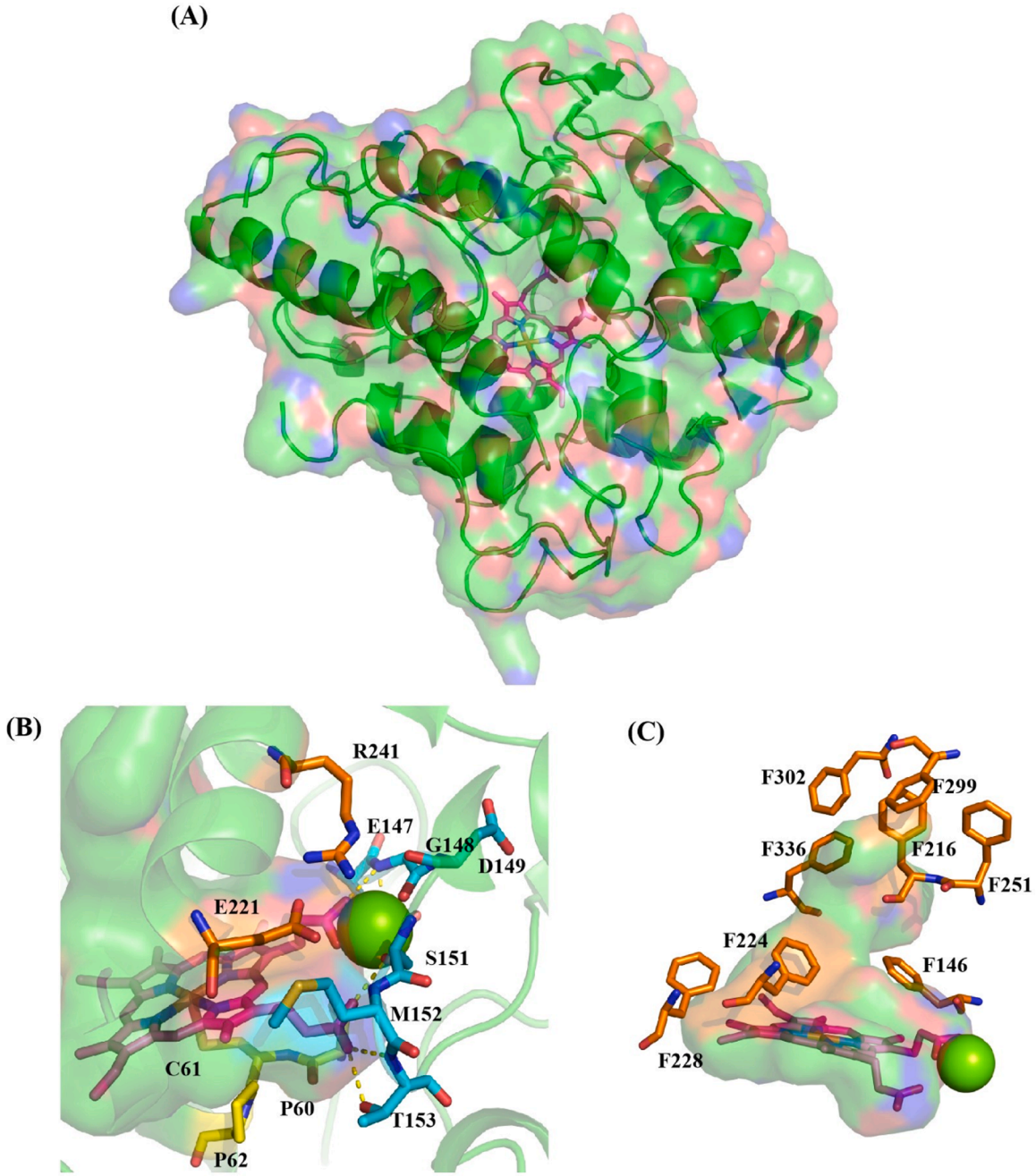

Fig. 2. Homology model of *Gma*UPO. (A): Overall structure of *Gma*UPO; (B): close-up on the active site with some catalytic/structural relevant residues highlighted: yellow: PCP motif (Pro60-Cys61-Pro62) providing the distal cysteine ligand for the heme prosthetic group; blue: EGD motif (Glu147-Gly148-Asp149) and SMT motif (Ser151-Met152-Thr153) stabilizing the heme moiety and coordinating the magnesium ion; orange: the catalytic diade (Glu221-Arg214) catalyzing the dehydratation of Cpd 0 to Cpd I; (C): highlighting the phenylalanine amino acids.

(Agilent Technologies, Palo Alto, CA, USA) outfitted with a J&W CP-Chirasil-Dex CB column (25 m length × 0.32 mm I.D. × 0.25 μm film thickness), and an FID detector. Injection volume: 1 μL; injection temperature: 250°C; split ratio: (30:1); detector temperature: 280°C. Cyclohexene and its products were detected by method B, whereas all other substrates and products (except fatty acids) were detected by method A. Using internal standard curves, measurements were obtained from peak areas. **Table S3** shows the retention times of various compounds

Method A: The oven was heated from 50°C to 130°C (2 min hold) by 10°C /min, 3°C/min to 150°C (1 min hold), 25°C/min to 200°C (2 min hold), 21.67 min total.

Method B: The oven was heated from 50°C to 130°C (2 min hold) by 5°C /min, 25°C/min to 200°C (1 min hold), 21.80 min total.

2.7. Gas chromatograph-mass spectrometry and temperature profiles

Fatty acid and product GC-MS analyses were performed on a Shimadzu TQ8050 Ultra (Shimadzu Technologies, Japan) equipped with Shimazu SH-Rxi-5Sil MS columns (30 m length × 0.25 mm I.D. × 0.25 μm film thickness), using He as carrier gas at a rate of 0.8 mL min^{-1}. split ratio (100:1), ion source temperature: 230°C, solvent delay time: 3 min. The oven was heated from 50°C (2 min hold) to 250°C (12 min hold) at a rate of 20°C /min for a total of 24 min. Total-ion peak areas were quantified using external standard curves and molar response factors of the same or similar compounds. **Table S4** shows the retention time of

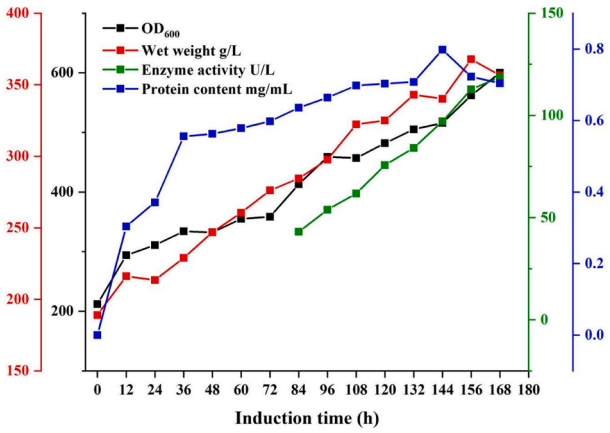

Fig. 3. Time course of the 7L-scale fermentation of *Pichia yeast* recombinantly expressing *Gma*UPO. Note that NBD-activity was not detectable until t = 72h.

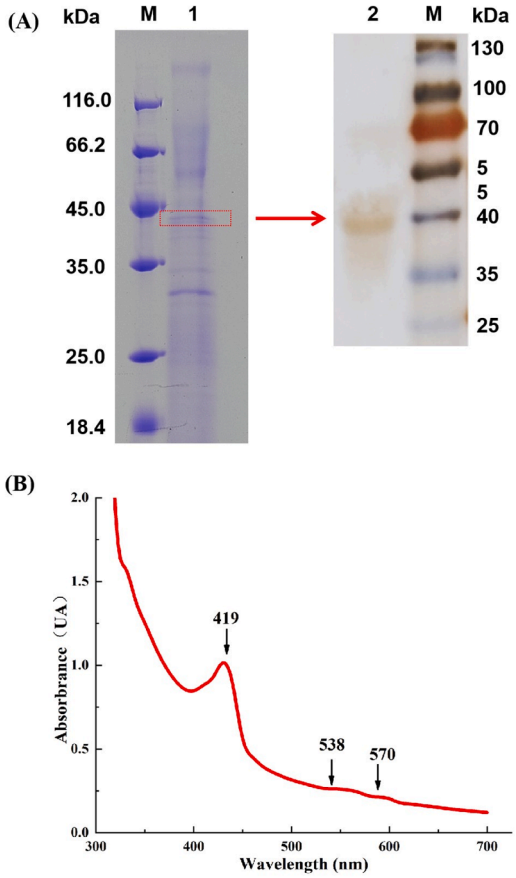

Fig. 4. SDS-PAGE (A left) and Western blot (A right) analysis of expression level of a *Gma*UPO expressed in *Pichia pastoris* X33 (M: Marker, 1 & 2: culture supernatant); (B): UV–Vis spectrum of *Gma*UPO highlighting the characteristic Soret band (419 nm) as well as the α- and β-bands (570 and 538, respectively).

various compounds.

2.8. Bioinformatic methods

2.8.1. Homologous modeling and molecular docking

Because the crystal structure of *Gma*UPO was not available, the homology model of *Gma*UPO was constructed using MODELLER program [47]. In the BLAST tool, *Gma*UPO exhibits 67.23% amino acid identity to *Aae*UPO (PDB ID: 5YOR). Therefore, the crystal structures of *Aae*UPO were used as templates to build the model of *Gma*UPO. The quality of the predicted model was estimated using PROCHECK [48], Verify 3D and ERRAT, respectively. The substrate (tridecanic acid) binding models of *Gma*UPO and *Aae*UPO were further constructed by molecular docking software AutoDock [49].

2.8.2. Generation of Cpd I, coordination residues, and substrate force field parameters

The force field parameters of Cpd I and coordination residues in *Gma*UPO and *Aae*UPO were obtained through the unbonded method of Metal Center Parameter Builder (MCPB) [50]. Structural optimization (**Figure S7**) and atomic charges were performed at the B3LYP/6-31G* (a system with 3 negative charges and 2 spin multiplicity). Meanwhile, force field parameters of tridecanic acid were derived from the AMBER GAFF force field [51] and their partial atomic charges were obtained from the restrained electrostatic potential (RESP) charge at the HF/6-31G (d) level with the Gaussian 09 package.

2.8.3. Construction of molecular dynamics simulation system

The protonation states of titrable amino acids in each enzyme molecule were determined by the Propka3 [48]. Their individual local hydrogen-bonding network was examined and then molecular dynamics simulations were conducted. Next, protonation was evaluated and each prepared model was neutralized by addition of Na^+ or Cl^- ions at the protein surface using the AmberTools package. Finally, it was solvated in a rectangular water box with a 10 Å buffer distance between the solvent box wall and the nearest solute atoms (water box models).

2.8.4. Classical molecular dynamics simulations

The classical molecular dynamics (CMD) process was performed as follows. First, the above-mentioned water box models and the H_2O_2 water box models were minimized to relax the solvent and optimize the system. A series of minimization were conducted and each model was heated from 0 to 300 K gradually under the NVT ensemble for 100 ps. This was followed by 150 ps of MD simulation under the NPT ensemble to relax the system density to about 1.0 g/cm^3 with a target temperature of 300 K and a target pressure of 1.0 atm. Subsequently, 100 ns of NVT MD simulation under periodic boundary conditions, target temperature of 300 K, and a time-step of 1.0 fs, was performed for each model to produce trajectories via the GPU accelerated pmemd program in the Amber 14 package. During the MD process, the TIP3P model and Amber99SB force field were applied for the water molecules and proteins, respectively [52–54]. The SHAKE algorithm was utilized to constrain all hydrogen-containing bonds with a tolerance of 10^{-5}. The Langevin dynamics method was used to control the system temperature with a collision frequency of 1.0 ps^{-1} (ntt = 3, gamma_ In = 1.0), and a cutoff of 12 Å was set for both van der Waals and electrostatic interactions.

In the constrained kinetics simulation, the distance (3.6 Å) between the Cpd I oxygen atom and the ω-1 carbon atom of tridecanoic acid in each model applied was 100 kcal·mol^{-1}·Å^{-2}.

2.8.5. Steered molecular dynamics simulation

The model of last frame of the classical dynamics simulation was selected as the initial structure of steered molecular dynamics (SMD) simulation. Using 10 kcal·mol^{-1}·Å^{-2} force, the ω-1 carbon atom of tridecanoic acid was pulled to the position of 3.3 Å from the Cpd I oxygen atom. The distance between the ω-1 carbon atom of tridecanoic acid and the Cpd I oxygen atom was set to the reaction coordination (RC) and the energy variation curve with the reaction coordinate driving method.

3. Results and Discussion

3.1. Bioinformatics analysis

The hypothetical UPO gene identified in the genome of *Galerina*

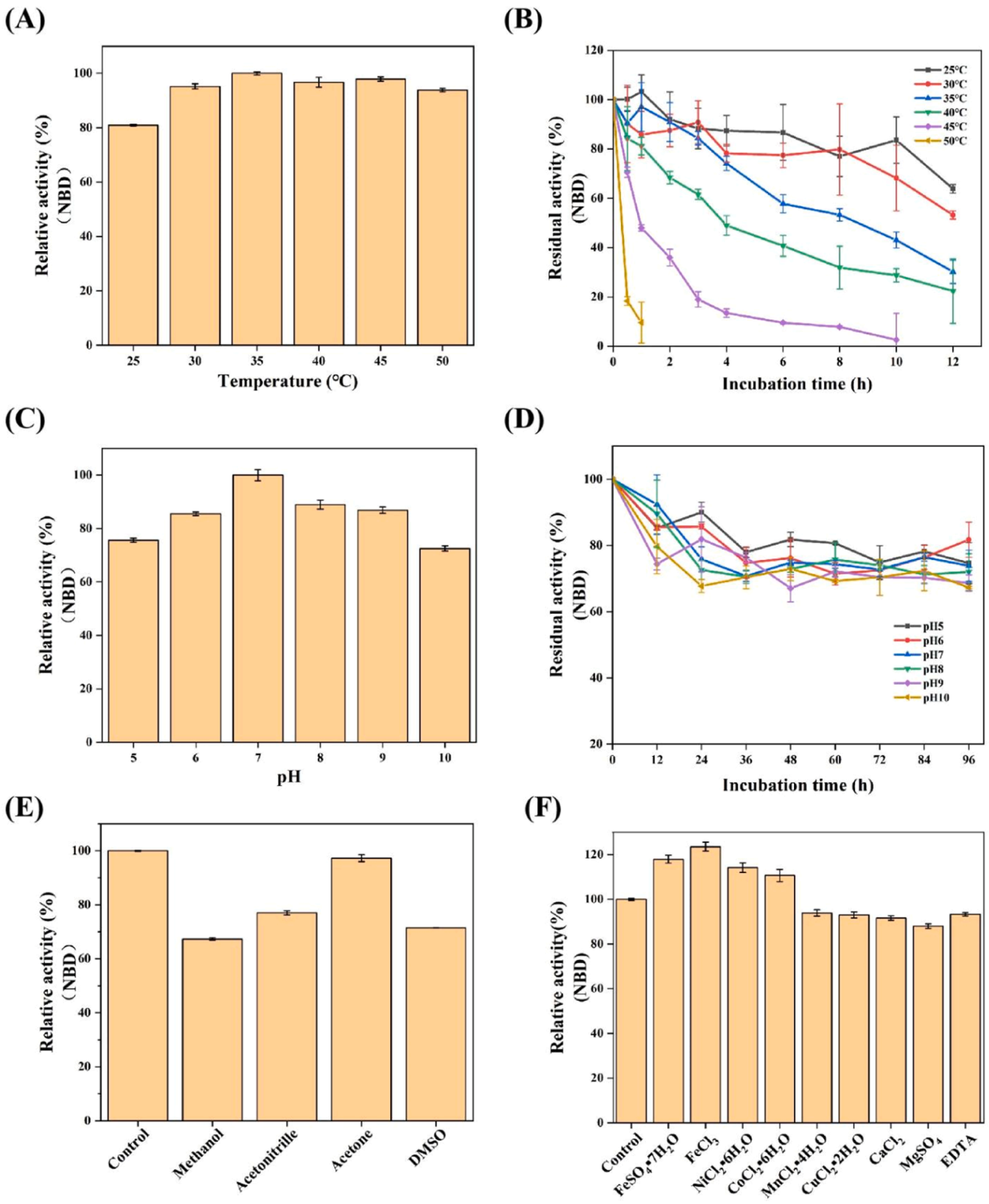

Fig. 5. Temperature (A-B), pH-(C-D) dependency of *Gma*UPO activity and -stability and effects of organic reagents solvents (E), metal ions (F) on the activity of *Gma*UPO

marginata (*Gma*UPO) was selected from the recently established peroxygenase database (UPObase). *Gma*UPO shows 67.23% identity with the well-known *Aae*UPO (**Figure S1 and Table S2**). It has a theoretical molecular weight of 38.27 kDa, an isoelectric point of 5.09, and an average total overall hydrophilicity coefficient of -0.244 (**Figure S2**). *Gma*UPO had a ProtScale-derived instability coefficient of 24.96, indicating that it should be stable under physiological conditions.

The secondary structure features of *Gma*UPO were examined using the SOPMA tool [55], which indicated a total of 12 α-helices, 2 β-sheets, and one disulfide bond (Cys61-Cys323) (Figure 2). The protein is made up of 34.56% α-helices, 5.95% short β-sheets, 11.33% extension band, and 48.16% random coil. We developed a homology model of *Gma*UPO using the crystal structure of *Aae*UPO as a template (Figure 2**A**). A closer look at the substrate access route above the heme catalytic moiety uncovered 8 phenylalanine residues (Figure 2**B**).

Overall, *Gma*UPO can be classified as a new member of the 'long-UPO' clade based on its high molecular weight, the presence of typical amino acid motifs, and the Phe-rich access channel [1].

Table 1
Preliminary evaluation of common UPO substrates for *Gma*UPO.

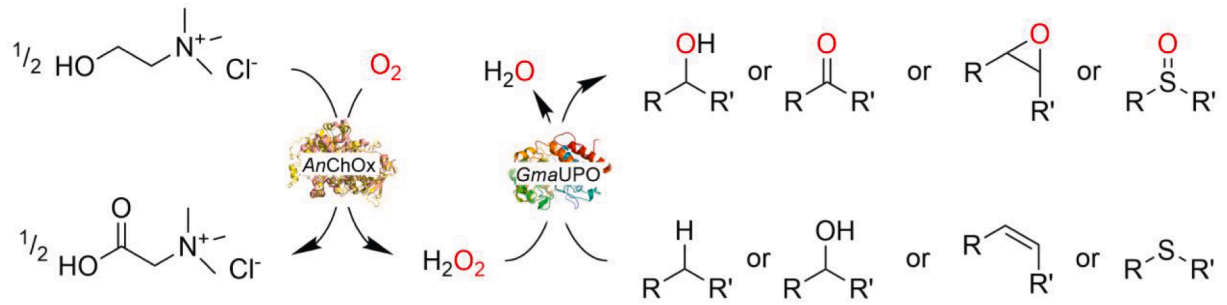

Substrate	Product	Product concentration [mM] / Conversion [%]	ee [%]
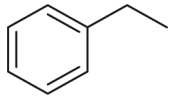	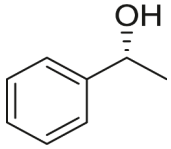	1.10 /11	64
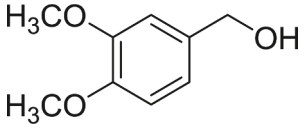	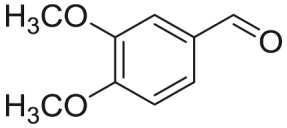	0.06/ 0.6	-
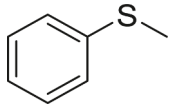	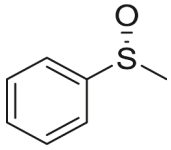	0.82 / 8.2	80
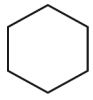	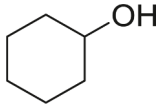	0.06 / 0.6	-
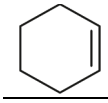	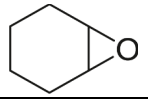	0.01 / 0.1	-

Reaction conditions: *Gma*UPO: 0.1U, ChCl (100mM), *An*ChOx (5μM) and substrate (10 mM) in NaPi buffer (50 mM, pH 7), V_{final} = 1 mL, 30°C, 500 rpm, 24 h. Product quantifications were obtained from peak areas, using internal standard curves. ee [%]= ([R]- [S])/([R]+[S]) × 100); conversion [%] = $([Product]_{final}/[Substrate]_0)$ × 100.

3.2. Preparation of GmaUPO

High-density fermentation of recombinant *Pichia pastoris* and expression of *Gma*UPO was realized in a 7-L bioreactor using pPICZαB-SP*gma-Gma*UPO/*Pichia.pastoris* X33. The supernatant protein content was 0.7 g/L, with a peroxygenase activity of 118 U/L (Figure 3). SDS-PAGE and western blot examination indicated the molecular mass of *Gma*UPO to be approximately 40 kDa (Figure 4), which is somewhat larger than the molecular weight determined from its gene sequence and is most likely owing to glycosylation of the polypeptide chains.

3.3. Biochemical characterization of GmaUPO

The effect of temperature on the rate of *Gma*UPO-catalyzed NBD-oxidation is shown in Figure 5**A-B**. Interestingly, *Gma*UPO activity did not appear to be affected by temperature within the experimental range (Figure 5**A**, 25°C < T < 50°C). However, the enzyme stability decreased with temperature (Figure 5**B**). While the enzyme at 25°C retained more than 60% of its initial activity after 12 h, it completely lost all activity after 1 h at 50°C.

Next, we investigated the effect of reaction pH on *Gma*UPO activity and stability. The pH profile of *Gma*UPO was fairly broad, with an optimum pH around 7 and more than 70% of this maximal activity at pH 5-10, respectively (Figure 5**C**). Similarly, pH had little effect on *Gma*UPO stability (Figure 5**D**).

Cosolvents are widely employed to improve the solubility of starting materials of interest in aqueous reaction environments because many of them are hydrophobic [56]. As a result, we investigated the effect of some common water-miscible organic solvents on *Gma*UPO activity (Figure 5**E**). Interestingly, the presence of approximately 30 % (v/v) methanol, acetonitrile, and DMSO lowered the catalytic activity of *Gma*UPO by less than 40%. Acetone had no discernible effect. Previously, similar observations were observed with *Aae*UPO [57], although *Hsp*UPO demonstrated significantly lower solvent tolerance [58]. We also looked into the effect of some common cations on *Gma*UPO activity. As shown in Figure 5**F**, Fe^{2+}, Fe^{3+}, Ni^{2+}, and Co^{2+} exhibited a minor activating effect, whereas other metal ions (Mn^{2+}, Cu^{2+}, Ca^{2+}, Mg^{2+}) and EDTA had no significant effect.

3.3.1. Substrate scope of GmaUPO

Finally, we performed an initial evaluation of the substrate and product scope of *Gma*UPO. As previously stated, H_2O_2 plays an ambiguous role as oxidant on the one hand but also as inactivator on the other hand. Therefore, to balance the *in situ* concentration of H_2O_2, we applied an enzymatic H_2O_2 generation system based on the choline oxidase-catalyzed oxidation of choline to betaine (Table 1).

*Gma*UPO exhibited a very similar reactivity pattern to *Aae*UPO, with the best substrates being ethyl benzene and thioanisol, albeit a somewhat lower enantioselectivity. The difference in enantioselectivity to *Aae*UPO represents a promising basis for the rationalization and,

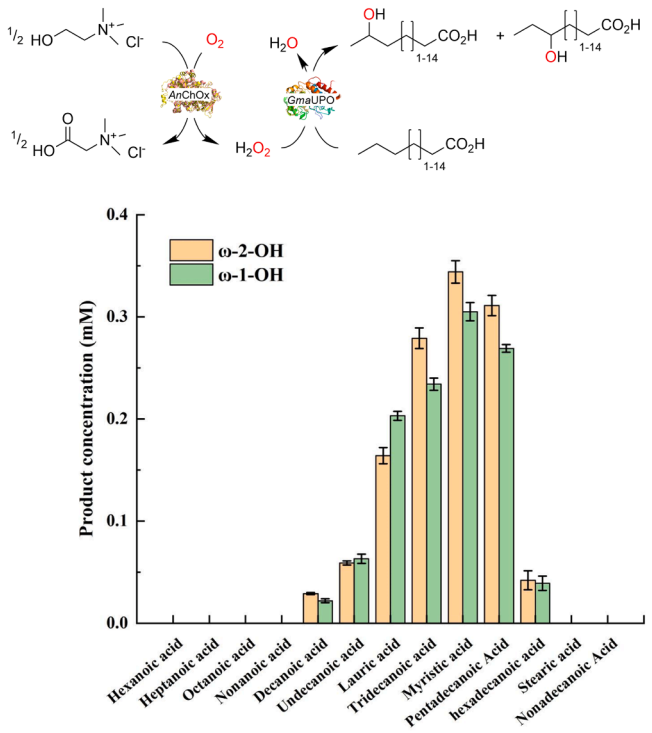

Fig. 6. *Gma*UPO-catalyzed oxyfunctionalization of selected fatty acids. Reaction conditions: *Gma*UPO: 0.1 U, ChCl (100 mM), *An*ChOx (5 μM) and substrate (1 mM) in NaPi buffer (50 mM, pH 7), V_{final} = 1 mL, 30°C, 500 rpm, 24h.

Fig. 7. 3D structure superposition of *Aae*UPO (rose red, PBD ID 5 YOR) and *Gma*UPO (green).

eventually, control over the enantioselectivity of *Aae*UPO- or *Gma*UPO-catalyzed oxyfunctionalization reactions. A detailed comparison of the active site structure of both enzymes may reveal amino acid residues relevant for enantioselectivity and thereby represent a good starting point for enzyme engineering.

Next, we investigated the activity of *Gma*UPO on fatty acids in some more detail. In general, fatty acids with chain lengths of 8 and higher were converted well with an apparent optimum around C10 (decanoic acid). The regioselectivity of *Gma*UPO was ω-1 and ω-2 C-H bonds with a slight preference for the ω-1 position (Figure 6).

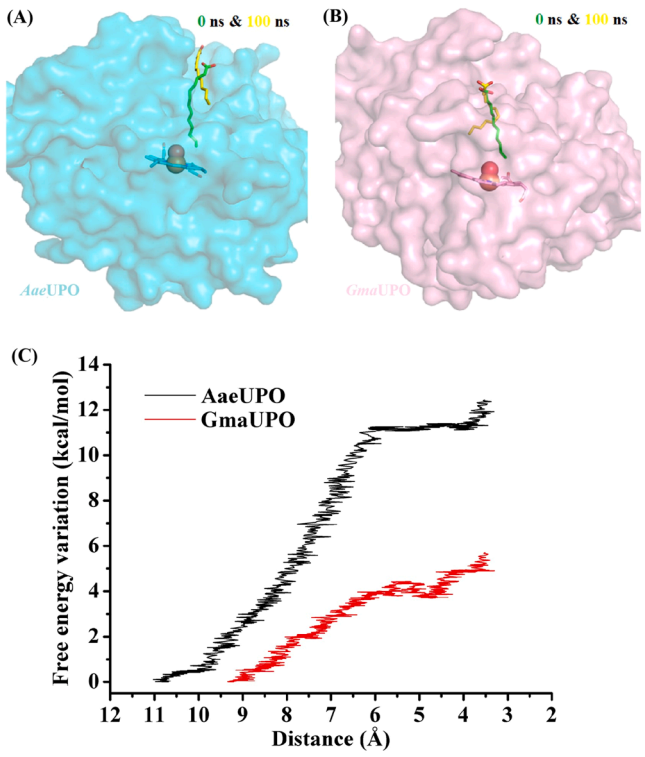

Fig. 8. A schematic showing *Aae*UPO, *Gma*UPO, and tridecanoic acid substrate molecule docking results (A-B) and the free energy variation of the tridecanoic acid ω-1 carbon gradually approaches the UPO Cpd I oxygen (C).

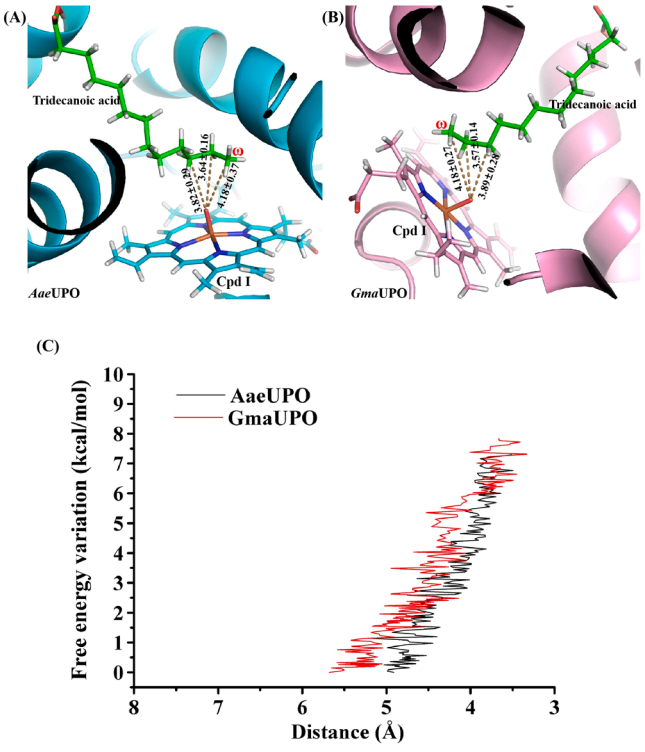

Fig. 9. A schematic showing the distance between the Cpd I oxygen atom of UPO and ω-1, ω-2, ω-3 carbon of tridecanoic acid in each UPO when the binding conformation of the three(A-B) and the free energy variation of the tridecanoic acid ω-1 carbon gradually approach the UPO Cpd I oxygen (C).

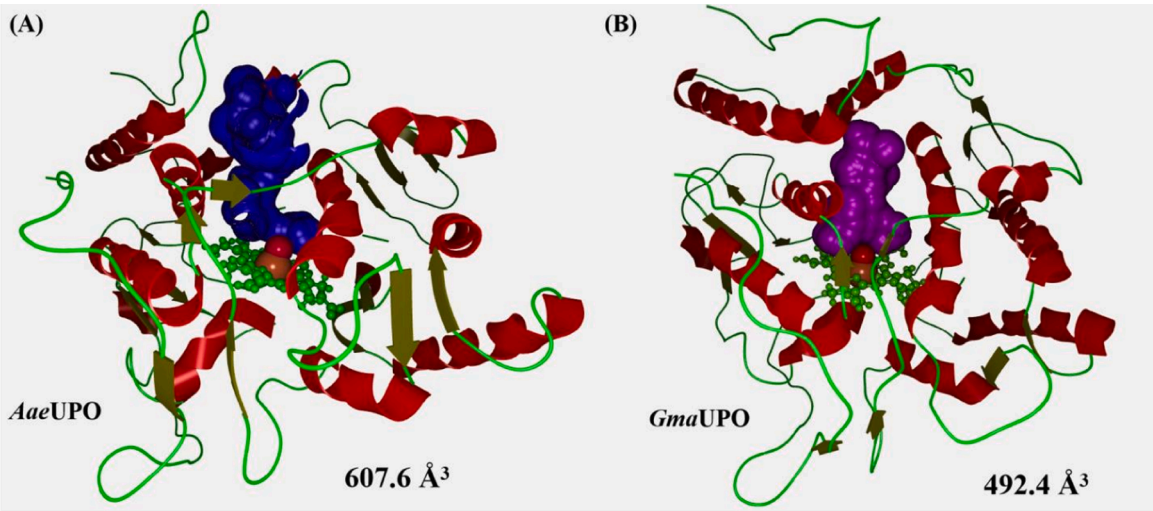

Fig. 10. Morphological analysis of *Aae*UPO (A) and *Gma*UPO (B) catalytic channel

Overall, the product spectrum of *Gma*UPO resembled the scope of *Aae*UPO [59], which, considering that both enzymes belong to the subclass of 'long UPOs' does not appear too astonishing.

3.4. Mechanism of position selectivity of fatty acid oxidation catalyzed by GmaUPO

Finally, we compared *Gma*UPO to the well-characterized *Aae*UPO to gain greater insight into the structural basis of its regioselectivity, particularly with fatty acids. The three-dimensional structures of *Aae*UPO and *Gma*UPO were superimposed, indicating that both enzymes have a high structural congruence (Figure 7).

3.4.1. Combination and reaction process of UPO and tridecanoic acid

Firstly, the substrate (tridecanoic acid)-enzyme complexes of *Gma*UPO and *Aae*UPO were constructed by molecular docking. Both, in *Aae*UPO and *Gma*UPO models, the fattya acids spontaneously migrated away from Cpd I oxygen atoms and the substrate stably attached to the catalytic channel entrance after 100 ns MD simulation (Figure 8 **A-B**). The results revealed that the fatty acid substrates thermodynamically tended to bind to the entrances of the two UPOs. Steer dynamics simulations (SMD) were used to elucidate the substrate trajectory and fluctuations in the energy level of fatty acid from outside the pocket to close to Cpd I. The energy level for the ω-1 position migrating closer to Cpd I increased to ~11.5 and ~5.0 kcal/mol in case of *Aae*UPO and *Gma*UPO, respectively (Figure 8 **C**).

3.4.2. On the regioselectivity difference in fatty acid oxidation catalyzed by UPOs

The constraint MD simulations of *Aae*UPO and *Gma*UPO were performed to better understand the regioselectivity of fatty acid hydroxylation. In guided dynamics, the conformation with a spacing of 3.6 Å between the ω-1 position carbon atom of tridecanoic acid and the Cpd I oxygen atom was selected as the initial model. The binding conformations of the two UPOs with the substrate reached equilibrium after 10 ns MD simulation. At this time, the distances between the Cpd I oxygen atom and the ω, ω-1, and ω-2 carbon atoms in *Gma*UPO were 4.18 ± 0.27, 3.57 ± 0.14 and 3.89 ± 0.28Å, respectively (Figure 9 **B**). The distance between *Aae*UPO and *Gma*UPO was comparable (Figure 9 **A**). Thus, *Gma*UPO and *Aae*UPO were more inclined to react with fatty acid substrates ω-1 and ω-2 C-H groups, demonstrating ω-1 and ω-2 selectivity.

The ω-3 of tridecanoic acid linked to *Aae*UPO and *Gma*UPO is being dragged closer to the oxygen atom of Cpd I via SMD. The free energy change curve demonstrates that the process is also not thermodynamically susceptible, with energy barriers of 7.5 and 8.0 kcal/mol, respectively (Figure 9 **C**). This shows how difficult it is to maintain contact with the carbon atom at the front end of the substrate and how difficult it is for Cpd I to react with the C-H group following the ω-2 carbon atom.

The analysis of catalytic cavity geometry revealed that both *Gma*UPO and *Aae*UPO have a large catalytic pocket (volumes of 492.4 and 607.6 $Å^3$, respectively) and their cavities connected environment and Cpd I directly (Figure 10). Compared to *Gma*UPO, the substrate channel of *Aae*UPO was narrower, resulting in a higher energy barrier from the meeting process between the substrate and Cpd I.

4. Conclusion

Admittedly, there are still many questions worthy of further in-depth study. One of the most important goals will be to optimize the expression conditions to improve the *Gma*UPO yield. Also structural characterization based on a crystal structure is currently ongoing. Here, especially the selectivity differences to *Aae*UPO will provide valuable structure-selectivity insights.

The currently low conversions are a direct consequence of the low expression levels and resulting low biocatalyst concentrations. Together with improved H_2O_2 provision systems, we expect that higher conversions and product titers will be attainable.

Nevertheless, with the current contribution we have added another UPO to the toolbox which will contribute to the development of new, more selective UPO mutants as practical tools for organic synthesis.

5. Author Contribution Statement

Yunjian Ma and Hongjing Liang conceived, designed the study, and performed the experiments, Zexin Zhao, Bin Wu analyzed the experimental data. Frank Hollmann assisted in data interpretation and manuscript formulation. Dongming Lan, Frank Hollmann and Yonghua Wang designed and directed the whole project. All the authors contributed to scientific discussion. The article was written based on contributions from all authors.

Declaration of Competing Interest

The authors declare that they have no known competing financial interests or personal relationships that could have appeared to influence the work reported in this paper.

Data Availability

Data will be made available on request.

Acknowledgements

This work was supported by the Key Program of Natural Science Foundation of China (31930084), National Natural Science Foundation of China (32001633), Guangzhou Science and technology planning project (202102020370), Key Realm R&D Program of GuangDong Province (2022B0202050003), National Outstanding Youth Science Foundation of China (31725022) and Macau Young Scholars Program (AM2020024).

Supplementary materials

Supplementary material associated with this article can be found, in the online version, at doi:10.1016/j.mcat.2022.112707.

References

[1] M. Hobisch, D. Holtmann, P.G. de Santos, M. Alcalde, F. Hollmann, S. Kara, Recent developments in the use of peroxygenases–exploring their high potential in selective oxyfunctionalisations, Biotechnol. Adv. 51 (2021), 107615.
[2] Y. Wang, D. Lan, R. Durrani, F. Hollmann, Peroxygenases en route to becoming dream catalysts. What are the opportunities and challenges? Curr. Opin. Chem. Biol. 37 (2017) 1–9.
[3] M. Hofrichter, R. Ullrich, Oxidations catalyzed by fungal peroxygenases, Curr. Opin. Chem. Biol. 19 (2014) 116–125.
[4] J. Münch, P. Püllmann, W. Zhang, M.J. Weissenborn, Enzymatic hydroxylations of sp3-carbons, ACS Catal. 11 (2021) 9168–9203.
[5] V.B. Urlacher, M. Girhard, Cytochrome P450 monooxygenases in biotechnology and synthetic biology, Trends Biotechnol. 37 (2019) 882–897.
[6] R.J. Li, Z. Zhang, C.G. Acevedo-Rocha, J. Zhao, A. Li, Biosynthesis of organic molecules via artificial cascade reactions based on cytochrome P450 monooxygenases, Green Synth. Catal. 1 (2020) 52–59.
[7] Y. Wei, E.L. Ang, H. Zhao, Recent developments in the application of P450 based biocatalysts, Curr. Opin. Chem. Biol. 43 (2018) 1–7.
[8] D.R. Morris, L.P. Hager, I. Chloroperoxidase, Isolation and properties of the crystalline glycoprotein, J. Biol. Chem. 241 (1966) 1763–1768.
[9] P.D. Shaw, L.P. Hager, Biological chlorination: VI. Chloroperoxidase: a component of the β-ketoadipate chlorinase system, J. Biol. Chem. 236 (1961) 1626–1630.
[10] A.T. Martínez, F.J. Ruiz-Dueñas, A. Gutiérrez, J.C. del Río, M. Alcalde, C. Liers, R. Ullrich, M. Hofrichter, K. Scheibner, L. Kalum, Search, engineering, and applications of new oxidative biocatalysts, Biofuels Bioprod. Biorefin. 8 (2014) 819–835.
[11] K. Piontek, R. Ullrich, C. Liers, K. Diederichs, D.A. Plattner, M. Hofrichter, Crystallization of a 45 kDa peroxygenase/peroxidase from the mushroom *Agrocybe aegerita* and structure determination by SAD utilizing only the haem iron, Acta Cryst. 66 (2010) 693–698.
[12] M. Hofrichter, R. Ullrich, Heme-thiolate haloperoxidases: versatile biocatalysts with biotechnological and environmental significance, Appl. Microbiol. Biotechnol. 71 (2006) 276–288.
[13] R. Ullrich, M. Hofrichter, The haloperoxidase of the agaric fungus *Agrocybe aegerita* hydroxylates toluene and naphthalene, FEBS Lett. 579 (2005) 6247–6250.
[14] R. Ullrich, J. Nüske, K. Scheibner, J. Spantzel, M. Hofrichter, Novel haloperoxidase from the agaric basidiomycete *Agrocybe aegerita* oxidizes aryl alcohols and aldehydes, Appl. Environ. Microbiol. 70 (2004) 4575–4581.
[15] A. Beltrán-Nogal, I. Sánchez-Moreno, D. Méndez-Sánchez, P.G. de Santos, F. Hollmann, M. Alcalde, Surfing the wave of oxyfunctionalization chemistry by engineering fungal unspecific peroxygenases, Curr. Opin. Struct. Biol. 73 (2022), 102342.
[16] E. Aranda, M. Kinne, M. Kluge, R. Ullrich, M. Hofrichter, Conversion of dibenzothiophene by the mushrooms *Agrocybe aegerita* and *Coprinellus radians* and their extracellular peroxygenases, Appl. Microbiol. Biotechnol. 82 (2009) 1057–1066.
[17] G. Gröbe, R. Ullrich, M.J. Pecyna, D. Kapturska, S. Friedrich, M. Hofrichter, K. Scheibner, High-yield production of aromatic peroxygenase by the agaric fungus *Marasmius rotula*, AMB Express 1 (2011) 1–11.
[18] A. Yarman, G. Gröbe, B. Neumann, M. Kinne, N. Gajovic-Eichelmann, U. Wollenberger, M. Hofrichter, R. Ullrich, K. Scheibner, F.W. Scheller, The aromatic peroxygenase from *Marasmius rutola*—a new enzyme for biosensor applications, Anal. Bioanal. Chem. 402 (2012) 405–412.
[19] R. Ullrich, M. Poraj-Kobielska, S. Scholze, C. Halbout, M. Sandvoss, M.J. Pecyna, K. Scheibner, M. Hofrichter, Side chain removal from corticosteroids by unspecific peroxygenase, J. Inorg. Biochem. 183 (2018) 84–93.
[20] J. Kiebist, K. Schmidtke, J. Zimmermann, H. Kellner, N. Jehmlich, R. Ullrich, D. Zänder, M. Hofrichter, K. Scheibner, A peroxygenase from *Chaetomium globosum* catalyzes the selective oxygenation of testosterone, ChemBioChem 18 (2017) 563–569.
[21] A. González-Benjumea, J. Carro, C. Renau-Mínguez, D. Linde, E. Fernández-Fueyo, A. Gutiérrez, A.T. Martínez, Fatty acid epoxidation by *Collariella virescens* peroxygenase and heme-channel variants, Catal. Sci. Technol. 10 (2020) 717–725.
[22] P. Molina-Espeja, S. Ma, D.M. Mate, R. Ludwig, M. Alcalde, Tandem-yeast expression system for engineering and producing unspecific peroxygenase, Enzym. Microb. Technol. 73 (2015) 29–33.
[23] P. Molina-Espeja, E. Garcia-Ruiz, D. Gonzalez-Perez, R. Ullrich, M. Hofrichter, M. Alcalde, Directed evolution of unspecific peroxygenase from *Agrocybe aegerita*, Appl. Environ. Microbiol. 80 (2014) 3496–3507.
[24] F. Tonin, F. Tieves, S. Willot, A. van Troost, R. van Oosten, S. Breestraat, S. van Pelt, M. Alcalde, F. Hollmann, Pilot-scale production of peroxygenase from *Agrocybe aegerita*, Org. Process Res. Dev. 25 (2021) 1414–1418.
[25] J. Martin-Diaz, P. Molina-Espeja, M. Hofrichter, F. Hollmann, M. Alcalde, Directed evolution of unspecific peroxygenase in organic solvents, Biotechnol. Bioeng. 118 (2021) 3002–3014.
[26] J. Ramirez-Ramirez, J. Martin-Diaz, N. Pastor, M. Alcalde, M. Ayala, Exploring the role of phenylalanine residues in modulating the flexibility and topography of the active site in the peroxygenase variant PaDa-I, Int. J. Mol. Sci. 21 (2020) 5734.
[27] P.G. de Santos, S. Lazaro, J. Viña-Gonzalez, M.D. Hoang, I. Sánchez-Moreno, A. Glieder, F. Hollmann, M. Alcalde, Evolved peroxygenase–aryl alcohol oxidase fusions for self-sufficient oxyfunctionalization reactions, ACS Catal. 10 (2020) 13524–13534.
[28] P. Molina-Espeja, P. Santos-Moriano, E. García-Ruiz, A. Ballesteros, F.J. Plou, M. Alcalde, Structure-guided immobilization of an evolved unspecific peroxygenase, Int. J. Mol. Sci. 20 (2019) 1627.
[29] P.G. de Santos, F.V. Cervantes, F. Tieves, F.J. Plou, F. Hollmann, M. Alcalde, Benchmarking of laboratory evolved unspecific peroxygenases for the synthesis of human drug metabolites, Tetrahedron 75 (2019) 1827–1831.
[30] J. Martin-Diaz, C. Paret, E. García-Ruiz, P. Molina-Espeja, M. Alcalde, Shuffling the neutral drift of unspecific peroxygenase in Saccharomyces cerevisiae, Appl. Environ. Microbiol. 84 (2018) 00808–00818.
[31] P.G. de Santos, M. Cañellas, F. Tieves, S.H.H. Younes, P. Molina-Espeja, M. Hofrichter, F. Hollmann, V. Guallar, M. Alcalde, Selective synthesis of the human drug metabolite 5′-hydroxypropranolol by an evolved self-sufficient peroxygenase, ACS Catal. 8 (2018) 4789–4799.
[32] P. Molina-Espeja, P.G. de Santos, M. Alcalde, Directed Evolution of Unspecific Peroxygenase, in: Directed Enzyme Evolution: Advances and Applications, Springer, 2017, pp. 127–143.
[33] P. Molina- Espeja, M. Cañellas, F.J. Plou, M. Hofrichter, F. Lucas, V. Guallar, M. Alcalde, Synthesis of 1- naphthol by a natural peroxygenase engineered by directed evolution, ChemBioChem 17 (2016) 341–349.
[34] D. Linde, A. Olmedo, A. González-Benjumea, M. Estévez, C. Renau-Mínguez, J. Carro, E. Fernández-Fueyo, A. Gutiérrez, A.T. Martínez, Two new unspecific peroxygenases from heterologous expression of fungal genes in Escherichia coli, Appl. Environ. Microbiol. 86 (2020) 02899. -02819.
[35] J. Carro, A. González-Benjumea, E. Fernández-Fueyo, C. Aranda, V. Guallar, A. Gutiérrez, A.T. Martínez, Modulating fatty acid epoxidation vs hydroxylation in a fungal peroxygenase, ACS Catal. 9 (2019) 6234–6242.
[36] P. Püllmann, M.J. Weissenborn, Improving the heterologous production of fungal peroxygenases through an episomal *Pichia pastoris* promoter and signal peptide shuffling system, ACS Synth. Biol. 10 (2021) 1360–1372.
[37] A. Knorrscheidt, J. Soler, N. Hünecke, P. Püllmann, M. Garcia-Borràs, M. J. Weissenborn, Accessing chemo-and regioselective benzylic and aromatic oxidations by protein engineering of an unspecific peroxygenase, ACS Catal. 11 (2021) 7327–7338.
[38] A. Knorrscheidt, J. Soler, N. Hünecke, P. Püllmann, M. Garcia-Borràs, M. J. Weissenborn, Simultaneous screening of multiple substrates with an unspecific peroxygenase enabled modified alkane and alkene oxyfunctionalisations, Catal. Sci. Technol. 11 (2021) 6058–6064.
[39] P. Püllmann, A. Knorrscheidt, J. Münch, P.R. Palme, W. Hoehenwarter, S. Marillonnet, M. Alcalde, B. Westermann, M.J. Weissenborn, A modular two yeast species secretion system for the production and preparative application of unspecific peroxygenases, Commun. Biol. 4 (2021) 1–20.
[40] A. Knorrscheidt, P. Püllmann, E. Schell, D. Homann, E. Freier, M.J. Weissenborn, Identification of novel unspecific peroxygenase chimeras and unusual YfeX axial heme ligand by a versatile high-throughput GC-MS approach, ChemCatChem 12 (2020) 4788–4795.
[41] X. Sang, F. Tong, Z. Zeng, M. Wu, B. Yuan, Z. Sun, X. Sheng, G. Qu, M. Alcalde, F. Hollmann, A Biocatalytic platform for the synthesis of enantiopure propargylic alcohols and amines, Org. Lett. 24 (2022) 4252–4257.
[42] M. Faiza, S. Huang, D. Lan, Y. Wang, New insights on unspecific peroxygenases: superfamily reclassification and evolution, BMC Evol. Biol. 19 (2019) 1–19.
[43] M. Poraj-Kobielska, M. Kinne, R. Ullrich, K. Scheibner, M. Hofrichter, A spectrophotometric assay for the detection of fungal peroxygenases, Anal. Biochem. 421 (2012) 327–329.
[44] Y. Ma, P. Li, Y. Li, S.J. Willot, W. Zhang, D. Ribitsch, Y.H. Choi, R. Verpoorte, T. Zhang, F. Hollmann, Natural deep eutectic solvents as multifunctional media for the valorization of agricultural wastes, ChemSusChem 12 (2019) 1310–1315.
[45] D. Ribitsch, S. Winkler, K. Gruber, W. Karl, E. Wehrschütz-Sigl, I. Eiteljörg, P. Schratl, P. Remler, R. Stehr, C. Bessler, Engineering of choline oxidase from Arthrobacter nicotianae for potential use as biological bleach in detergents, Appl. Microbiol. Biotechnol. 87 (2010) 1743–1752.
[46] D. Ribitsch, W. Karl, E. Wehrschütz-Sigl, S. Tutz, P. Remler, H.J. Weber, K. Gruber, R. Stehr, C. Bessler, N. Hoven, Heterologous expression and characterization of

choline oxidase from the soil bacterium Arthrobacter nicotianae, Appl. Microbiol. Biotechnol. 81 (2009) 875–886.
[47] N. Eswar, M.A. Marti Renom, B. Webb, MS Madhusudhan, D. Eramian, M. Shen, U. Pieper, A Sali, Com parative protein structure modeling with Modeller, Curr. Protoc. Bioinform. 15 (2006) 5–6.
[48] M.H.M. Olsson, C.R. Søndergaard, M. Rostkowski, J.H. Jensen, PROPKA3: consistent treatment of internal and surface residues in empirical p K a predictions, J. Chem. Theory. Comput 7 (2011) 525–537.
[49] G.M. Morris, R. Huey, W. Lindstrom, M.F. Sanner, R.K. Belew, D.S. Goodsell, A. J. Olson, AutoDock4 and AutoDockTools4: automated docking with selective receptor flexibility, J. Comput. Chem. 30 (2009) 2785–2791.
[50] P. Li, K.M. Merz Jr, MCPB. py: a python based metal center parameter builder, J. Chem. Inform. Model. 56 (2016) 599–604.
[51] J. Wang, R.M. Wolf, J.W. Caldwell, P.A. Kollman, D.A. Case, Development and testing of a general amber force field, J Comput. Chem. 25 (2004) 1157–1174.
[52] W.D. Cornell, P. Cieplak, C.I. Bayly, I.R. Gould, K.M. Merz, D.M. Ferguson, D. C. Spellmeyer, T. Fox, J.W. Caldwell, P.A. Kollman, A second generation force field for the simulation of proteins, nucleic acids, and organic molecules, J. Am. Chem. Soc. 117 (1995) 5179–5197.
[53] V. Hornak, R. Abel, A. Okur, B. Strockbine, A. Roitberg, C. Simmerling, Comparison of multiple Amber force fields and development of improved protein backbone parameters, Proteins Struct. Funct. Bioinform. 65 (2006) 712–725.
[54] J. Wang, P. Cieplak, P.A. Kollman, How well does a restrained electrostatic potential (RESP) model perform in calculating conformational energies of organic and biological molecules? J. Comput. Chem. 21 (2000) 1049–1074.
[55] C. Combet, C. Blanchet, C. Geourjon, G. Deleage, NPS@: network protein sequence analysis, Trends. Biochem. Sci. 25 (2000) 147–150.
[56] M.M.C.H. van Schie, J.D. Spöring, M. Bocola, P.D. de María, D. Rother, Applied biocatalysis beyond just buffers–from aqueous to unconventional media. Options and guidelines, Green Chem. 23 (2021) 3191–3206.
[57] T. Hilberath, A. van Troost, M. Alcalde, F. Hollmann, Assessing peroxygenase-mediated oxidations in the presence of high concentrations of water-miscible co-solvents, Front. Catal. 2 (2022), 882992, https://doi.org/10.3389/fctls.2022.882992.
[58] L. Rotilio, A. Swoboda, K. Ebner, C. Rinnofner, A. Glieder, W. Kroutil, A. Mattevi, Structural and biochemical studies enlighten the unspecific peroxygenase from Hypoxylon sp. EC38 as an efficient oxidative biocatalyst, ACS Catal. 11 (2021) 11511–11525.
[59] A. Gutiérrez, E.D. Babot, R. Ullrich, M. Hofrichter, A.T. Martínez, C. José, Regioselective oxygenation of fatty acids, fatty alcohols and other aliphatic compounds by a basidiomycete heme-thiolate peroxidase, Arch. Biochem. Biophys. 514 (2011) 33–43.